Journal of Corrosion and Materials
www.corromat.com

J. Corros. Mater. (2025) 4(2), 220–229.

A Confinement-Sensitive Crack-Width Model for Bond Deterioration in Marine-Corroded Reinforced Concrete: Calibration, Thresholds, and Residual-Capacity Screening

Amable Liñán Martínez[1,*]

Department of Fluid Mechanics and Aerospace Propulsion, ETSI Aeronáutica y del Espacio, Universidad Politécnica de Madrid, Plaza Cardenal Cisneros 3, 28040 Madrid, Spain

[*]Corresponding author: amable.linan@upm.es

(Received: 29 August 2025. Received in revised form: 26 November 2025. Accepted: 8 December 2025. Published online: 30 December 2025.)

Abstract

Bond degradation at the steel–concrete interface is a primary driver of serviceability loss and capacity reduction in marine-exposed reinforced concrete (RC), and it can become critical even when the reduction in steel area remains comparatively moderate. While accelerated-corrosion pull-out experiments have established strong empirical correlations between bond strength and corrosion-induced cracking, engineering practice still lacks a simple and actionable inspection-to-capacity mapping that converts measurable surface crack width into bond retention and residual-capacity screening. This paper develops a confinement-sensitive, crack-width–based bond deterioration model calibrated from reported pull-out test data for RC cube specimens with deformed bars of 16–25 mm diameter under severe simulated marine corrosion, considering both unconfined and stirrup-confined detailing. We propose (i) an exponential crack-width law for unconfined members, (ii) a piecewise "no-loss" regime followed by exponential decay for confined members, and (iii) practical crack-width thresholds corresponding to target bond-retention levels (90%, 70%, and 50%). A simple residual-capacity screening relationship is then introduced to translate bond retention into residual strength ratio for preliminary assessment and maintenance prioritization. The resulting framework enables transparent, inspection-driven decision support for corroded marine RC elements, and it is readily extensible to field monitoring and reliability-based updating as new data become available.

Keywords: reinforced concrete, marine corrosion, bond strength, confinement, crack width, pull-out test, deterioration model, residual capacity, maintenance thresholds.

1. Introduction

Reinforced concrete (RC) is the dominant construction material for coastal and offshore infrastructure because of its constructability, stiffness, and favorable life-cycle cost [1, 2]. However, in aggressive marine exposure zones—particularly the splash and tidal regions—RC durability is governed by chloride transport through the cover, depassivation of reinforcing steel, and the subsequent initiation and propagation of corrosion [3, 4]. Chloride ingress occurs through a combination of capillary suction, wetting–drying cycles, diffusion, and permeation, with local acceleration due to cracking, construction joints, and inadequate cover [5, 6]. Once the chloride concentration at the steel surface exceeds a critical threshold, the passive film breaks down and corrosion reactions produce voluminous rust products [7, 8]. These corrosion products occupy substantially larger volume than the consumed steel and generate expansive pressures at the steel–concrete interface. The resulting tensile hoop stresses in the surrounding concrete promote longitudinal splitting cracks along the bar and, at more advanced stages, delamination and spalling of the cover [9]. In marine members subjected to repeated wetting and drying, this damage can develop non-uniformly along the reinforcement, leading to localized bond deterioration even when the average loss of steel area appears modest.

The integrity of the steel–concrete bond is central to the composite action assumed in RC design [10]. Bond mechanisms include chemical adhesion at early loading stages, mechanical interlock between deformed bar ribs and the surrounding concrete, and frictional resistance mobilized by radial confinement. Corrosion perturbs each mechanism. First, corrosion alters the rib geometry and may reduce effective rib height and bearing area, weakening mechanical interlock. Second, the accumulation of corrosion products changes the interface conditions: at early stages, rust layers and increased roughness can sometimes transiently increase frictional resistance, whereas at later stages, cracking and loss of confinement dominate and bond resistance collapses [2, 6]. Third, and most critically for structural performance, corrosion-induced splitting cracks reduce the radial confining stress that is needed to prevent splitting failure. As confinement deteriorates, the bond response shifts from a ductile pull-out mechanism toward brittle splitting, increasing slip at lower load levels and reducing stiffness and strength. These bond losses propagate to member-level consequences: larger crack spacing and widths, reduced tension stiffening, increased deflection, reduced anchorage and lap-splice reliability, and compromised load transfer in regions where bond demand is high (development lengths, beam-column joints, and shear-critical zones).

Although a substantial experimental literature has established that corrosion degrades bond through (i) reduction and alteration of rib geometry, (ii) accumulation of rust products at the interface, and (iii) cracking of the cover that reduces confinement, the translation of these findings into inspection practice remains limited [10]. Field assessments commonly document visible cracking, rust staining, and spalling, and they may supplement these observations with electrochemical indicators such as half-cell potential, resistivity, or corrosion-rate estimates [8]. However, maintenance decisions are often driven by qualitative crack surveys or by simplified corrosion proxies rather than by a calibrated relationship linking measurable surface damage to bond capacity. This limitation is important because corrosion penetration or mass loss is difficult to estimate accurately without intrusive testing and because corrosion is spatially heterogeneous. In contrast, surface crack width is a readily observable indicator that directly reflects the internal expansion pressures and the associated loss of confinement [9]. For large inventories of marine RC elements (wharves, piers, piles, dolphins, and coastal retaining structures), where access can be constrained and inspection resources are limited, a transparent and quantitative mapping from crack width to bond retention would provide an immediate benefit: it would support consistent condition ranking, enable rapid screening for prioritization, and offer a defensible basis for triggering more detailed evaluations.

Existing predictive approaches for bond deterioration under corrosion often rely on corrosion level, bar cross-section loss, or empirical reduction factors embedded in design guidance [7]. While informative, these approaches are not always compatible with typical inspection outputs and may not explicitly distinguish confinement regimes. In practice, confinement varies widely across marine structures: some members include closely spaced stirrups or ties that maintain radial restraint, whereas others (e.g., lightly confined slabs, older piles, or regions with deteriorated cover) may behave as effectively unconfined once splitting initiates [11]. Because confinement strongly controls the transition from limited degradation to rapid bond loss, a deterioration law that explicitly incorporates confinement in a simple way is attractive for field use. Furthermore, decision-making requires thresholds: engineers need to know not only that "bond decreases with crack width," but also approximately what crack widths correspond to meaningful capacity reductions (e.g., 90%, 70%, or 50% bond retention) under different detailing conditions.

This paper addresses these needs by developing a confinement-sensitive crack-width deterioration model calibrated from reported accelerated-corrosion pull-out experiments on RC cube specimens with and without stirrup confinement and with multiple bar diameters [10]. The central objective is to provide an interpretable, evidence-based relationship between a measurable field quantity (surface crack width) and bond retention. Specifically, the paper (i) formulates a parsimonious crack-width law for unconfined specimens, (ii) introduces a piecewise confined model with an explicit "no-loss" regime followed by controlled decay, and (iii) derives practical crack-width thresholds that correspond to target bond-retention levels suitable for maintenance screening. The proposed framework is intended as a rapid, transparent screening tool to support inspection-to-action decisions and to complement—rather than replace—detailed nonlinear analysis and member-specific assessment when critical regions or high-demand scenarios are identified.

2. Dataset, experimental context, and crack-width calibration

The present work is a secondary analysis and model calibration based on reported accelerated-corrosion pull-out experiments conducted on reinforced concrete (RC) cube specimens representative of marine-exposed deterioration mechanisms [11,12]. The objective of this section is to (i) document the experimental context and the variables extracted for calibration, (ii) define a consistent set of normalized response measures suitable for cross-comparison across bar diameters and detailing, and (iii) introduce and calibrate confinement-sensitive crack-width laws that map directly to bond retention and maintenance-relevant thresholds.

The calibration dataset is taken from pull-out tests on 200 mm cube specimens containing a single centered deformed reinforcing bar of diameter $d_b \in 16, 20, 25$ mm. Two detailing configurations were reported: an unconfined configuration without transverse reinforcement, and a confined configuration incorporating 8 mm stirrups at 40 mm spacing. The reported embedment length was $L_e = 150$ mm and the nominal concrete cover was approximately 50 mm. Corrosion was accelerated in a 5% NaCl electrolyte using an impressed-current technique intended to reproduce the dominant mechanical consequence of marine reinforcement corrosion, namely the formation of corrosion products at the steel–concrete interface and the resulting splitting damage in the cover concrete [13]. After the target corrosion exposure, specimens were subjected to pull-out testing, and the following quantities were reported at the specimen level: surface crack width, corrosion level (e.g., mass loss/penetration proxy), rust mass, and peak bond stress.

Although impressed-current acceleration does not replicate all aspects of natural corrosion (e.g., macrocell effects, moisture gradients, and long-term transport processes), it is widely used to isolate the structural mechanics of corrosion-induced cracking and to produce measurable gradients of damage within practical laboratory durations [14]. For the present purpose, the accelerated protocol is leveraged as a calibration basis for an inspection-oriented model that links an observable field indicator (crack width) to bond retention.

Let $P_{\max}$ denote the measured peak pull-out load (when reported), and let τ denote the corresponding average bond stress at peak. When the original study reports τ directly, those values are adopted. When only $P_{\max}$ is provided, the bond stress is consistently defined using the classical uniform-average relation

$$\tau = \frac{P_{\max}}{\pi d_b L_e}, \tag{1}$$

where d_b is the bar diameter and L_e is the embedment length. Because absolute bond strength depends on bar diameter, concrete strength, and confinement, a normalized measure is required to isolate the corrosion-induced deterioration trend and to enable a unified crack-width mapping. Accordingly, for each diameter and detailing class, let τ_0 denote the corresponding uncorroded control bond strength. The *bond retention ratio* is then defined as

$$r = \frac{\tau}{\tau_0}, \tag{2}$$

so that $r = 1$ represents the undamaged reference state and $r \to 0$ indicates severe bond deterioration.

Let w denote the measured surface crack width in mm, interpreted as the representative longitudinal splitting crack width attributed to corrosion-induced expansion. Additional reported explanatory variables include a corrosion level proxy (e.g., average corrosion penetration or mass loss fraction) and rust mass. These variables are useful for mechanistic interpretation, but crack width is adopted as the primary predictor in this study because it is (i) directly observable during inspection, (ii) strongly coupled to loss of confinement, and (iii) more straightforward to measure at scale than corrosion penetration or mass loss, which typically require intrusive verification or specialized electrochemical inference.

The central modeling goal is therefore to determine a practical and confinement-sensitive mapping

$$r = r(w), \tag{3}$$

with parameters calibrated separately for unconfined and confined cases and with thresholds w_p that satisfy $r(w_p) = p$ for maintenance-relevant retention targets p.

Across the reported specimen set, bond retention exhibits a clear decreasing trend with increasing crack width, with the most pronounced degradation in the unconfined configuration where splitting cracks directly reduce radial restraint and promote brittle splitting-type failure. Similar qualitative monotonic behavior is observed for bond versus corrosion level and bond versus rust mass. Nevertheless, both corrosion level and rust mass are less directly accessible in routine inspection workflows, and they can vary spatially along the bar length in ways that are not captured by a single scalar estimate. Crack width, by contrast, is a surface manifestation of the internal expansion pressure and associated confinement loss, and it naturally aggregates local damage processes that control bond capacity. For screening applications, it is therefore preferable to place crack width at the center of the deterioration law.

A parsimonious functional form is also essential. Over the observed crack-width range, an exponential decay model provides a stable monotone mapping, allows straightforward calibration by log-linear regression, and yields closed-form threshold crack widths for target retention levels. Importantly, confinement modifies the early-stage response: for confined specimens, the reported results support a short regime in which bond retention remains near unity for very small cracks, followed by controlled decay once splitting damage becomes sufficient to reduce effective confinement. This motivates a piecewise form for the confined case.

For unconfined specimens, bond retention is modeled using an exponential deterioration law:

$$r_{\mathrm{U}}(w) = \exp(-k_{\mathrm{U}}\, w)\,, \tag{4}$$

where $k_{\mathrm{U}} > 0$ is a decay parameter in mm^{-1}. Calibrating Eq. (4) to the reported unconfined dataset yields

$$k_{\mathrm{U}} \approx 3.31\ \ \mathrm{mm}^{-1}, \tag{5}$$

which provides low residual error for screening purposes over the reported crack-width range.

For confined specimens, a "no-loss" regime is introduced to reflect the fact that transverse reinforcement can maintain radial restraint despite incipient splitting. The following piecewise model is adopted:

$$r_{\mathrm{C}}(w) = \begin{cases} 1, & w \le w_0, \\ \exp(-k_{\mathrm{C}}(w - w_0))\,, & w > w_0, \end{cases} \tag{6}$$

where w_0 is a confinement-controlled threshold crack width and k_{C} is the post-threshold decay parameter. Using the reported confinement behavior (negligible reduction up to approximately $w \sim 0.006$ mm) and fitting to the confined dataset yields

$$w_0 \approx 0.006\ \mathrm{mm}, \qquad k_{\mathrm{C}} \approx 7.68\ \mathrm{mm}^{-1}. \tag{7}$$

Eq. (6) captures the key structural feature that confinement delays the onset of measurable bond loss and then governs the subsequent decay as cracking progresses.

Table 1: Calibrated crack-width model parameters for bond retention.

Detailing	Model	Threshold w_0 (mm)	Decay parameter (mm^{-1})
Unconfined	$r_U(w) = \exp(-k_U w)$	–	$k_U = 3.31$
Confined	Eq. (6)	$w_0 = 0.006$	$k_C = 7.68$

For transparency and reproducibility, Figure 1 is included as a recommended visualization: a scatter plot of r versus w separated by detailing class, overlaid with the calibrated curves from Eqs. (4)–(6). This figure is particularly useful in demonstrating the confinement-dependent transition from near-unity retention to degradation.

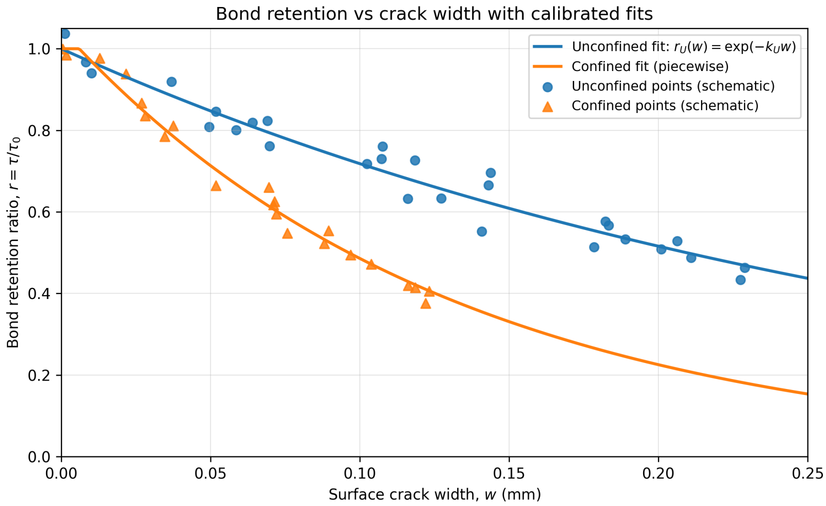

Figure 1: Recommended plot for calibration presentation: bond retention $r = \tau/\tau_0$ versus crack width w, separated by unconfined and confined detailing, with fitted models from Eqs. (4)–(6).

To support rapid screening, define threshold crack widths w_p as those satisfying $r(w_p) = p$ for target retention levels $p \in \{0.90, 0.70, 0.50\}$. These targets correspond to common screening questions: whether bond capacity remains largely intact (near 90%), whether deterioration is moderate and warrants detailed evaluation (around 70%), and whether severe degradation is plausible and intervention planning is justified (near 50%).

For unconfined specimens (Eq. (4)),

$$w_p^U = -\frac{\ln(p)}{k_U}. \tag{8}$$

For confined specimens (Eq. (6)) with $p < 1$,

$$w_p^C = w_0 - \frac{\ln(p)}{k_C}. \tag{9}$$

Table 2: Crack-width thresholds (mm) for target bond retention levels, based on calibrated models.

Detailing	$w_{0.90}$	$w_{0.70}$	$w_{0.50}$
Unconfined (Eq. (4), k_U=3.31)	0.032	0.108	0.209
Confined (Eq. (6), w_0=0.006, k_C=7.68)	0.020	0.052	0.096

Table 2 provides a direct inspection-to-retention mapping. In the unconfined case, crack widths on the order of 0.10 mm correspond to a transition toward substantial bond loss under the calibrated law, while crack widths near 0.20 mm indicate the potential for severe degradation. In the confined case, the fitted model reflects a delayed onset of deterioration through w_0, after which the decay parameter governs the rate of bond reduction; the resulting thresholds remain practically small, underscoring that even with transverse reinforcement, corrosion-induced splitting can quickly erode bond once cracking becomes visible and propagates. These thresholds are intended for screening and prioritization and should be paired with member-specific evaluation when high demand regions (development lengths, splices, joints) or critical structural roles are present.

The calibrated relationships in this section are intentionally compact and are aimed at providing an interpretable, field-compatible deterioration mapping. The parameters in Table 1 are context-informed values derived from the reported dataset and should be regarded as screening coefficients rather than universal constants. The framework is designed to be extensible: additional datasets spanning different cover depths, concrete strengths, stirrup ratios, or natural exposure histories can be incorporated by recalibrating k_{U}, w_0, and k_{C}, or by introducing modest diameter dependence when sufficient data supports it. Within the present scope, the normalized retention formulation in Eq. (2) offers a practical basis for translating measured crack widths into bond retention and maintenance thresholds without requiring invasive corrosion quantification.

3. Residual-capacity screening and inspection-to-action workflow

Corrosion-induced bond deterioration affects structural performance through multiple coupled mechanisms. At the material-interface level, reduced bond strength and stiffness increase bar slip and degrade tension stiffening, which in turn enlarges crack widths and crack spacing, increases deflection, and accelerates localization of damage. At the member level, bond deterioration compromises anchorage and lap splice performance, reduces the effective development of reinforcement stress, and can shift governing failure modes toward brittle splitting or premature pull-out. These effects are particularly consequential in marine RC elements where bond demand is elevated in development zones, beam–column joints, pile heads, and regions with high shear transfer and cyclic action. Because detailed nonlinear analyses and destructive verification are not feasible for large inventories, a practical framework is needed to convert inspection-observable indicators into a conservative, first-pass estimate of residual capacity for prioritization.

To bridge the gap between interface-level deterioration and structural decision-making, we introduce a screening relationship between bond retention and a member-level residual strength ratio. Let $r = \tau/\tau_0$ denote the bond retention ratio as defined previously, where τ is the peak average bond stress and τ_0 is the corresponding uncorroded reference value. Define the *residual strength ratio* R as the ratio of the estimated current structural capacity to the nominal uncorroded capacity for a given performance metric of interest (e.g., peak load capacity, moment capacity, or a serviceability-based limit state):

$$R = \frac{C_{\mathrm{dam}}}{C_0}, \tag{10}$$

where C_{dam} is the capacity under corrosion damage and C_0 is the undamaged baseline. In general, R depends on multiple deterioration contributors (steel area loss, reduced yield strength in extreme cases, reduced concrete cover confinement due to spalling, and bond degradation). For rapid screening, the focus here is to capture the leading-order influence of bond deterioration through an explicit, interpretable mapping from r to R.

A simple linear model is adopted:

$$R \approx a + b\,r, \tag{11}$$

where a represents the residual strength fraction not explained by bond retention alone (e.g., contributions from alternative load paths or conservative baseline assumptions), and b represents the sensitivity of structural capacity to bond retention. Using reported residual strength percentages for representative unconfined and confined cases in the calibration source, the fitted coefficients yield a near-identity mapping:

$$a \approx 0.01, \qquad b \approx 0.99. \tag{12}$$

This result suggests that, within the considered experimental context and the reported residual-capacity interpretation, the residual strength ratio closely tracks bond retention. Consequently, a conservative first-pass screening approximation is:

$$R \approx r \qquad \text{(screening approximation).} \tag{13}$$

The practical value of Eq. (13) is that it enables an immediate translation from measured crack width (via $r(w)$) to a residual-capacity indicator without requiring intrusive corrosion quantification. The approximation is intentionally conservative and is not intended to replace member-specific assessment. In particular, member-level capacity may deviate from $R \approx r$ when (i) steel cross-section loss becomes dominant, (ii) severe cover spalling reduces compression-zone integrity or confinement, (iii) failure is governed by shear or joint behavior rather than anchorage, or (iv) cyclic and fatigue effects control deterioration. Nonetheless, as an inventory-level screening tool, the mapping provides a consistent and defensible method for ranking elements and triggering further evaluation.

For transparency, Figure 2 is recommended to accompany this section: a scatter plot of observed R versus computed r for all specimens where both metrics can be inferred, overlaid with the fitted line from Eq. (11) and the identity line $R = r$. If desired, a simple uncertainty band can be provided by adopting a conservative lower-envelope model:

$$R_{\mathrm{LB}} = \max\{0,\ a_{\mathrm{LB}} + b_{\mathrm{LB}} r\}, \tag{14}$$

with $(a_{\mathrm{LB}}, b_{\mathrm{LB}})$ chosen so that a high percentage (e.g., 90–95%) of points lie above R_{LB}. This provides a conservative decision rule even when scatter is present.

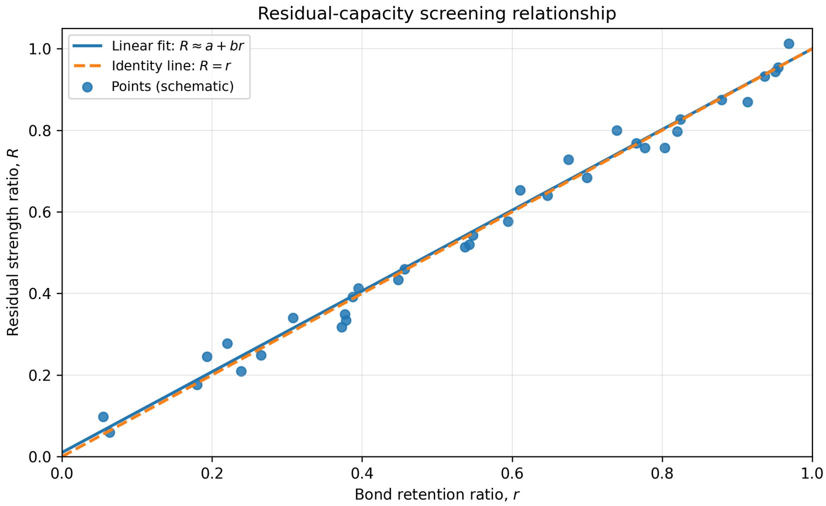

Figure 2: Recommended screening validation plot: residual strength ratio R versus bond retention ratio r with linear fit (Eq. (11)) and identity line $R = r$.

Combining the crack-width bond-retention model $r(w)$ with the residual-capacity screening relationship yields a practical inspection-to-action workflow for marine RC elements. The workflow is designed for field deployment across large inventories and emphasizes consistent data capture, conservative screening, and clear triggers for escalation. The steps are as follows.

First, conduct a condition survey and measure representative corrosion-induced crack widths w at structurally relevant locations, with emphasis on splash/tidal zones, pile heads, beam soffits near supports, lap splice regions, anchorage zones, and joints. Crack measurements should be paired with photographic documentation and notes on crack continuity, rust staining, and spall extent, as these observations help distinguish corrosion-driven splitting from other crack mechanisms.

Second, determine the effective confinement class. Even when transverse reinforcement is present, members may behave as effectively unconfined if cover spalling has occurred, if stirrups are widely spaced relative to bar diameter, or if cracking patterns indicate loss of radial restraint. Accordingly, classify each assessed region as (i) confined (intact cover with functioning transverse reinforcement) or (ii) effectively unconfined (no transverse reinforcement or confinement compromised by damage). When uncertainty exists, the unconfined model should be adopted for conservative screening.

Third, compute bond retention using the calibrated crack-width mapping:

$$r \;=\; r_{\mathrm{U}}(w) \;\;\text{or}\;\; r_{\mathrm{C}}(w), \tag{15}$$

using Eq. (4) for unconfined regions and Eq. (6) for confined regions. Fourth, map bond retention to residual capacity using Eq. (11) with calibrated coefficients or, conservatively, Eq. (13):

$$R \approx r. \tag{16}$$

Finally, apply maintenance-oriented triggers using the crack-width thresholds in Table 2 or equivalently in terms of r and R. A practical interpretation is to treat $r \geq 0.90$ as a condition compatible with routine monitoring, $0.70 \leq r < 0.90$ as a zone requiring increased inspection frequency and targeted diagnostic testing, and $r < 0.70$ as a trigger for engineering evaluation of development lengths, splices, and member capacity. When r approaches or falls below 0.50, the screening framework indicates a plausible risk of severe bond degradation, and intervention planning (repair, strengthening, load restriction, or replacement) should be prioritized subject to structural importance and redundancy.

The workflow is intentionally simple, but several implementation points improve robustness. Crack-width measurements should be taken as distributions (e.g., minimum/median/maximum) over a defined length, rather than as a single value, because corrosion damage is heterogeneous. When multiple cracks are present, the governing crack width should be used for conservative screening, while the median can be used for ranking across similar elements. The classification of confinement should consider the current condition of the cover and ties, not only original drawings. Finally, when screening identifies potentially critical deterioration, the model should be escalated to member-specific assessment incorporating (i) steel area loss, (ii) spalling and confinement degradation, and (iii) the governing structural demand in anchorage and splice regions. Despite these caveats, the combined $w \to r \to R$ mapping provides a consistent bridge from inspection measurements to capacity-informed prioritization, enabling rational allocation of limited maintenance resources across marine RC inventories.

4. Discussion

The proposed framework combines two intentionally compact mappings: a confinement-sensitive crack-width law for bond retention, $w \to r(w)$, and a screening translation from bond retention to residual strength ratio, $r \to R$ [15, 16]. This section interprets these relationships mechanistically, evaluates their practical implications for marine RC assessment, and delineates limitations and pathways for extension [17]. The discussion is structured around (i) physical meaning of crack width as a bond-damage proxy, (ii) the role of confinement and the transition between failure modes, (iii) implications of the calibrated thresholds for inspection and maintenance, (iv) interpretability and transferability to field conditions, and (v) uncertainty and model refinement [18].

A central premise of the paper is that surface crack width is an effective indicator of bond loss because it is a macroscopic manifestation of the same internal processes that reduce bond capacity [19]. Corrosion generates products with a larger specific volume than the consumed steel, creating expansive pressure at the interface and inducing tensile hoop stresses in the surrounding concrete [9, 20]. Once these hoop stresses exceed the tensile capacity of the cover, longitudinal splitting cracks form parallel to the reinforcement. These cracks are not merely a symptom of corrosion; they directly reduce the radial confining stress that enables mechanical interlock between the deformed ribs and the surrounding concrete [21]. As confinement decays, the resisting mechanism shifts from rib bearing with stable confinement to progressive splitting and rapid degradation in bond resistance [22].

In this sense, crack width is a damage-integrating variable: it reflects the combined effect of corrosion extent, rust distribution, concrete tensile capacity, cover depth, and the current confinement condition [23]. This contrasts with average corrosion penetration or mass loss, which are difficult to measure non-destructively and can be spatially non-uniform along the bar and across the member. In routine inspections, crack width can be repeatedly measured at low cost, making it compatible with asset management [24]. The proposed exponential forms exploit this practicality while maintaining a monotone, physically plausible relationship between increasing splitting severity and decreasing bond retention [25].

It is important to acknowledge that crack width is not a perfect proxy in all situations. Crack widths can be influenced by external loading, restraint conditions, temperature effects, and shrinkage, and multiple crack types may coexist [13]. Nonetheless, in marine environments, the presence of longitudinal cracks aligned with reinforcement, accompanied by rust staining and local delamination, is strongly suggestive of corrosion-induced splitting. The framework is intended for such corrosion-relevant cracking, and its use should be paired with basic crack classification to avoid misinterpretation of flexural or shrinkage cracks as corrosion splitting.

The distinction between unconfined and confined detailing is not a purely geometric label; it represents a fundamental difference in how the interface can sustain radial stresses during corrosion progression. In unconfined configurations, the cover provides the primary restraint. Once splitting initiates, confinement decreases rapidly because the cover cracks can open and propagate with limited resistance, allowing significant loss of bond at comparatively small crack widths. This is consistent with the calibrated unconfined decay parameter and the relatively larger threshold crack widths required to reach strong reductions in bond retention [16, 19].

In confined configurations, transverse reinforcement provides an alternative source of radial restraint, delaying the effective loss of confinement and stabilizing the bond mechanism in early stages. The piecewise confined model captures this through the introduction of a "no-loss" regime up to w_0, reflecting that very small cracks may not meaningfully reduce the confinement delivered by intact stirrups and unspalled cover [20]. Beyond this regime, the decay parameter controls the deterioration rate, representing progressive damage accumulation, possible stirrup corrosion interaction, and reduced effectiveness of confinement as cracks widen.

A key practical implication is that the confinement class should be interpreted as an *effective* condition rather than a nominal detailing attribute. A member originally detailed with stirrups may behave as effectively unconfined if spalling, delamination, or transverse reinforcement corrosion has compromised confinement. Conversely, a nominally unconfined configuration may exhibit partial restraint due to geometry, external compression, or surrounding structural continuity. For screening, adopting the unconfined model in ambiguous cases is conservative and aligns with the goal of preventing underestimation of degradation.

The derived crack-width thresholds provide an actionable translation of the fitted deterioration laws into decision-support quantities. The thresholds for $r = 0.90$, 0.70, and 0.50 can be interpreted as three levels of condition severity: near-intact bond, moderate deterioration requiring engineering attention, and severe deterioration plausibly associated with significant anchorage or splice risk [14]. Importantly, these thresholds are derived from normalized bond retention. Therefore, they are largely insensitive to the absolute bond strength level, which depends on concrete strength and bar diameter, and they are more transferable across similar materials than raw bond stress values.

From an inspection standpoint, the thresholds highlight that even relatively small corrosion-induced crack widths can correspond to meaningful bond loss, particularly when confinement is compromised. This reinforces a practical observation from marine infrastructure: the onset of longitudinal cracking often marks a transition to accelerated deterioration because it facilitates chloride ingress and creates direct transport pathways to reinforcement. Thus, the thresholds should be viewed not only as capacity indicators but also as durability indicators that may justify more frequent inspections and protective measures.

At the same time, crack-width thresholds should not be interpreted as universal acceptance criteria. They are screening triggers, and they must be contextualized by structural demand. For instance, a given bond retention ratio may be more critical in lap splice regions, anchorage zones, and joints than in midspan regions where bond demand is lower [13]. Therefore, a risk-informed application should couple the thresholds with knowledge of demand hotspots and redundancy. The workflow proposed in the paper supports this by directing measurements toward critical regions and by treating the screening outputs as prioritization cues rather than final capacity ratings.

The exponential form is attractive for screening for three reasons [15]. First, it enforces monotonicity and boundedness ($r \in (0, 1]$), matching the physical expectation that increasing splitting damage cannot increase bond capacity in the long run. Second, it yields closed-form thresholds and straightforward calibration. Third, it offers interpretability: the decay parameter has a clear meaning as the rate at which bond retention decreases with crack width. A more complex model could potentially reduce residual error, but it would risk overfitting to a limited dataset and reduce transparency for field use. The present approach emphasizes robustness and ease of deployment.

That said, the exponential form does not explicitly capture a possible early-stage frictional enhancement sometimes observed at very low corrosion levels before cracking occurs. The confined piecewise form partially addresses this by allowing a near-unity regime at small crack widths. For unconfined cases, the model is calibrated over crack widths where splitting damage is present and thus is aligned with the primary degradation regime of interest for inspection-based decisions.

The proposed relationship $R \approx a+br$ (with a near-identity fit) offers a pragmatic bridge from interface-level deterioration to an inventory-level residual-capacity indicator. The near-identity behavior suggests that, for the considered test context, bond retention captures a dominant portion of the capacity loss interpreted by the source study. This supports the operational approximation $R \approx r$ for rapid ranking.

However, the screening mapping should be interpreted carefully. Structural capacity is multi-mechanistic, and bond retention alone cannot capture all capacity reductions in all members. In advanced corrosion states, steel area loss may dominate, especially in tension-controlled flexural regions. In shear-critical members, corrosion-induced cracking and stirrup corrosion can reduce shear capacity disproportionately relative to bond retention [21–23]. In columns and piles, axial load interaction and confinement loss due to spalling may introduce additional reductions not directly reflected in pull-out bond capacity. Therefore, $R \approx r$ is most defensible as a conservative, preliminary indicator for prioritization and not as a substitute for design-level verification.

One beneficial feature is that the mapping encourages a consistent, quantitative narrative during triage: rather than relying on subjective labels (minor, moderate, severe), inspectors can estimate a residual ratio that is comparable across elements. This enables transparent prioritization in asset management, provided that criticality and demand are incorporated as additional filters.

The calibration is derived from cube pull-out specimens with a specific embedment length, cover depth, and accelerated corrosion protocol. Field members differ in geometry, restraint, loading state, moisture gradients, and long-term cracking histories. Several scale-related issues may therefore influence transferability.

First, crack width in real members is often influenced by sustained mechanical loading and restraint, which may superimpose on corrosion-induced splitting. Proper crack classification is essential, and ideally crack width measurements should focus on longitudinal cracks along reinforcement lines in zones where corrosion is suspected. Second, bond in real members is affected by casting position, bar spacing, concrete heterogeneity, and confinement from surrounding reinforcement cages. Third, natural corrosion is often non-uniform, producing pitting and localized damage that can create localized debonding not fully captured by average crack width measures.

Despite these differences, the proposed framework remains useful because it leverages normalization ($r = \tau/\tau_0$) and focuses on crack width as a damage-integrating indicator. In practice, the primary value is in *relative* ranking and in providing conservative triggers for escalation. For member-specific decisions, the model coefficients should ideally be updated using local calibration data (cores, pull-out tests, or field performance records) where available.

Uncertainty arises at multiple stages: crack-width measurement variability, heterogeneity of corrosion damage, differences between accelerated and natural corrosion, and scatter in bond test outcomes. Crack width itself is a random field along the member, and single-point measurements can underrepresent localized maxima. Therefore, a conservative practice is to record distributions (minimum/median/maximum) over a defined length and to use the governing value for screening when safety-critical.

Model-form uncertainty also exists: while the exponential law provides stable behavior, alternative monotone forms (e.g., logistic decay, power-law) could fit specific datasets slightly better. The priority here is not to achieve minimum error in a laboratory dataset but to provide a deployable decision-support mapping. A practical enhancement is to provide lower-bound curves (e.g., conservative envelopes) so that screening estimates err on the safe side. Incorporating such envelopes would also facilitate probabilistic updating in future work: crack width measurements can be treated as observations that update the distribution of r and thus R.

From a life-cycle perspective, the framework suggests that visible corrosion-induced cracking should be treated as a key transition point. Once cracks form, chloride ingress accelerates and the deterioration rate can increase, producing a coupled feedback between durability and structural capacity. The crack-width thresholds therefore provide a practical basis for defining inspection intervals and intervention triggers. For example, elements exhibiting crack widths associated with $r < 0.9$ may warrant more frequent monitoring and protective actions (coatings, cathodic protection assessment), whereas elements near or below the $r < 0.7$ level should be prioritized for engineering evaluation of anchorage and splice reliability and for repair planning.

Importantly, the framework supports prioritization at scale: even if the exact r value is uncertain, the model provides a consistent ordering that can be combined with criticality factors (traffic importance, redundancy, consequence of failure) to allocate limited maintenance resources.

The present work is a first step toward inspection-driven bond and capacity assessment. Several extensions can substantially increase its fidelity while preserving usability. First, introducing explicit dependence on cover depth-to-bar diameter ratio (c/d_b), stirrup ratio, and concrete strength would broaden applicability. Second, integrating electrochemical indicators (half-cell potential, resistivity) as auxiliary predictors could improve discrimination between corrosion-induced cracks and mechanically induced cracks [24,25]. Third, calibrating member-level relationships (beams, columns, piles) would refine the $r \to R$ mapping for different failure modes and demand regimes. Finally, adopting a Bayesian calibration would allow practitioners to update model parameters for a given asset class as field data accumulates, producing asset-specific deterioration curves and probabilistic thresholds.

Overall, the proposed crack-width–based deterioration model and residual-capacity screening translation offer a practical bridge from observable corrosion damage to engineering decision-making. The framework is intentionally transparent and conservative, positioning it as a useful triage tool for marine RC inventories and as a foundation for more detailed, data-rich reliability-based approaches.

5. Conclusions

This paper developed an inspection-oriented framework for evaluating bond deterioration and screening residual capacity of marine-corroded reinforced concrete by linking an easily measurable field indicator—surface crack width—to bond retention and a first-pass residual strength ratio. The main outcomes can be summarized as follows.

A confinement-sensitive crack-width deterioration model was proposed and calibrated using reported accelerated-corrosion pull-out data for RC cube specimens with 16–25 mm deformed bars, considering both unconfined and stirrup-confined detailing. For unconfined configurations, bond retention was represented by a compact exponential law, providing a stable monotone mapping from crack width to normalized bond strength. For confined configurations, a piecewise form captured the observed early-stage "no-loss" regime followed by controlled exponential decay, reflecting the role of transverse reinforcement in delaying effective confinement loss. Closed-form expressions were then derived to compute crack-width thresholds corresponding to target bond-retention levels (90%, 70%, and 50%), yielding practical triggers for condition ranking and maintenance prioritization.

References

[1] Neville, A. M. (1995). *Properties of Concrete* (Vol. 4, p. 1995). London: Longman.

[2] Mehta, P. K., & Monteiro, P. J. (2006). *Concrete Microstructure, Properties, and Materials*. McGraw-hill.

[3] Bertolini, L., Elsener, B., Pedeferri, P., Redaelli, E., & Polder, R. B. (2013). *Corrosion of Steel in Concrete: Prevention, Diagnosis, Repair.* John Wiley & Sons.

[4] Angst, U., Elsener, B., Larsen, C. K., & Vennesland, Ø. (2009). Critical chloride content in reinforced concrete—A review. *Cement and Concrete Research, 39*(12), 1122-1138.

[5] Pacheco, J., & Polder, R. (2011, November). Corrosion initiation and propagation in cracked concrete–a literature review. In *Advances in Modeling Concrete Service Life: Proceedings of 4th International RILEM PhD Workshop held in Madrid, Spain, November19, 2010* (pp. 85-93). Dordrecht: Springer Netherlands.

[6] Stanish, K. D., Hooton, R. D., & Thomas, M. D. A. (1997). Testing the chloride penetration resistance of concrete: a literature review.

[7] Tuutti, K. (1982). *Corrosion of Steel in Concrete.*

[8] Andrade, C., & Alonso, C. (1996). Corrosion rate monitoring in the laboratory and on-site. *Construction and Building Materials, 10*(5), 315-328.

[9] Alonso, C., Andrade, C., Rodriguez, J., & Diez, J. M. (1998). Factors controlling cracking of concrete affected by reinforcement corrosion. *Materials and Structures, 31*(7), 435-441.

[10] Shafto, M., Conroy, M., Doyle, R., Glaessgen, E., Kemp, C., LeMoigne, J., & Wang, L. (2010). Draft modeling, simulation, information technology & processing roadmap. *Technology Area, 11*, 1-32.

[11] Rodriguez, J., Ortega, L. M., & Casal, J. (1994, June). Corrosion of reinforcing bars and service life of reinforced concrete structures: corrosion and bond deterioration. In *International Conference on Concrete across borders, Odense, Denmark* (Vol. 2, pp. 315-326). Taylor & Francis, Abingdon, UK.

[12] Fang, C., Lundgren, K., Chen, L., & Zhu, C. (2004). Corrosion influence on bond in reinforced concrete. *Cement and Concrete Research, 34*(11), 2159-2167.

[13] Cabrera, J. G. (1996). Deterioration of concrete due to reinforcement steel corrosion. *Cement and Concrete Composites, 18*(1), 47-59.

[14] El Maaddawy, T. A., & Soudki, K. A. (2003). Effectiveness of impressed current technique to simulate corrosion of steel reinforcement in concrete. *Journal of Materials in Civil Engineering, 15*(1), 41-47.

[15] fib-federation internationale du beton. (2013). *Fib Model Code for Concrete Structures 2010.* John Wiley & Sons.

[16] Isgor, B., Halmen, C., Trejo, D., & Tepke, D. (2024, April). Recent Initiatives of ACI Committee 222 on Corrosion of Metals in Concrete. In *RILEM Spring Convention and Conference* (pp. 329-338). Cham: Springer Nature Switzerland.

[17] Broomfield, J. P. (2023). *Corrosion of Steel in Concrete: Understanding, Investigation and Repair.* Crc Press.

[18] Bertolini, L., Elsener, B., Pedeferri, P., Redaelli, E., & Polder, R. B. (2013). *Corrosion of Steel in Concrete: Prevention, Diagnosis, Repair.* John Wiley & Sons.

[19] Lundgren, K. (2005). Bond between ribbed bars and concrete. Part 2: The effect of corrosion. *Magazine of Concrete Research, 57*(7), 383-395.

[20] Lau, I. (2024). *Time-Dependent Reliability Analysis of Corrosion-Induced Concrete Cracking Based on Fracture Mechanics Criteria* (Doctoral dissertation, RMIT University).

[21] Eligehausen, R., Popov, E. P., & Bertero, V. V. (1983). Local bond stress-slip relationships of deformed bars under generalized excitations: experimental results and analytical model.

[22] Auyeung, Y., Balaguru, P., & Chung, L. (2000). Bond behavior of corroded reinforcement bars. *Materials Journal, 97*(2), 214-220.

[23] Coronelli, D., & Gambarova, P. (2004). Structural assessment of corroded reinforced concrete beams: modeling guidelines. *Journal of Structural Engineering, 130*(8), 1214-1224.

[24] ACI Committee. (2001). *Guide to Durable Concrete.* American Concrete Institute.

[25] Adasooriya, N. D., Samarakoon, S., & Gudmestad, O. T. (2018). Corrosion propagation phase and bond strength degradation of reinforced concrete structures: State of the art. *Materials Characterisation, 47.*